cles with the atmosphere where the dipole field line enters it can be obtained from the directional variations in the particle fluxes. We determined relative directional fluxes of particles using counting rates in the E2 and P2 channels (Fig. 3) and the simultaneously measured magnetic field (5). The directional fluxes varied considerably with decreasing radial distance from the planet, becoming increasingly anisotropic closer to the planet. Thus, only particles whose velocity vectors have large angles relative to the local magnetic field can remain trapped at the closer distances.

The electron flux profile in Fig. 1B is similar to that deduced previously from Pioneer 11 measurements during its closest approach to the planet (*10*). The earlier Pioneer 11 profile was shown, in turn, to be consistent (for certain assumptions about the electron energy spectra and about nonradiative losses) with ground-based measurements of the jovian decimetric radio emissions (*14*). The data from the probe E2 electron coincidence channel are within a factor of 3 of previous Pioneer levels in the region where there is overlap. Examination of the electron spectra indicates that relatively more higher-energy as compared to lower-energy particles were measured with the probe instrument than reported from the Pioneer missions for the same energy range.

VAREFERENCES AND NOTES

1. B. F. Burke and K. L. Franklin, *J. Geophys. Res.* **60**, 213 (1955).
2. Special issue on Pioneer 10, *Science* **183** (1974); special issue on Pioneer 10, *J. Geophys. Res.* **79** (1974).
3. H. M. Fischer *et al.*, *Space Sci. Rev.* **60**, 1 (1992). The EPI detector assembly consists of a two-element telescope that uses totally depleted, circular silicon surface barrier detectors. Each detector has a thickness of 0.5 mm, a radius of 1.4 mm, and a sensitive area of 6.2 mm^2. A 3-mm-thick (equivalent to 2.55 g cm^{-2}) brass absorber is inserted between the two detectors in order to expand the energy range of particles that can be measured. The total length of the telescope (upper surface front detector to lower surface back detector) is 6 mm. The detector assembly is surrounded by tungsten shielding with a cylindrical wall thickness of 2.7 mm (equivalent to 4.86 g cm^{-2}). The entire probe and its contents, estimated to be equivalent to at least 80 g cm^{-2}, form the rear shielding of the telescope. A number of instrument performance effects during flight—such as acceptance curves for energy channels, final geometrical factors, deadtime losses, stray coincidences, and multiparticle events, as well as the influence of the heat shield—are accounted for here only with initial estimates. The instrument temperature during the encounter was <0°C, so no thermal noise problems existed in the detectors.
4. For the E1, E2, and E3 electron thresholds in Table 1, the tabulated values are obtained from range-energy relations. When the scattering of incident electrons from the aft heat shield is considered, the median energies detected by these thresholds, based on Monte Carlo transport calculations, correspond to higher energies that depend on the energy spectrum of the incident electrons. The E2, P2, P3, He, and HV measurements use coincidence detections between the two solid-state detectors.
5. L. J. Lanzerotti *et al.*, *Science* **272**, 858 (1996).
6. The HV channel may be dominated in some regions by interactions of energetic He with the telescope structure. We determined the fluxes using nominal geometrical factors and efficiencies. The geometrical factors used are 0.18 and 0.246 cm^2 sr for (E1 and P1) and (E2, P2, P3, He, and HV), respectively.
7. K. R. Pyle, R. B. McKibben, J. A. Simpson, *J. Geophys. Res.* **88**, 45 (1983); R. B. McKibben, K. R. Pyle, J. A. Simpson, *ibid.*, p. 36.
8. R. W. Fillius, C. E. McIlwain, A. Mogro-Campero, *Science* **188**, 465 (1975).
9. J. H. Trainor, F. B. McDonald, D. E. Stilwell, B. J. Teegarden, W. R. Webber, *ibid.*, p. 462.
10. J. A. Van Allen *et al.*, *ibid.*, p. 465.
11. F. B. McDonald and J. H. Trainor, in *Jupiter*, T. Gehrels, Ed. (Univ. of Arizona Press, Tucson, AZ, 1976), p. 961.
12. J. A. Simpson and R. B. McKibben, *ibid.*, p. 738.
13. D. C. Jewitt and E. Danielson, *J. Geophys. Res.* **86**, 8691 (1981).
14. I. dePater and C. K. Goertz, *ibid.* **95**, 39 (1990).
15. E. Pehlke, thesis, Institut für Kernphysik, Universität Kiel, Germany (1988).

16. We thank the NASA Ames Galileo Project Office, B. Chin, A. Wilhelmi, C. Sobeck, M. Smith, R. Young, and the technical staff for assistance during the long interval of excellent cooperation. We are grateful to F. Gliem and J. Bach (University of Braunschweig); F. Wendler, P. Glasow, and G. Eberlein (Siemens Company, Erlangen, Germany); the technical staff of the Dornier-System Company (Friedrichshafen, Germany); and the technical and administrative staff of VARTA Battery Company (Kelkheim and Hannover, Germany) for their help in making the LRD-EPI instrument a success. Thanks are due to E. Böhm (University of Kiel) for his contributions in scientific discussions and his assistance in data evaluation and with programs for particle track simulations in the detector telescope; S. Sievers (University of Kiel) for his help with the figures; and J. A. Van Allen (University of Iowa) for helpful suggestions. The EPI investigations were supported by the German Agency for Space Activities DARA by grant number 50 QJ 9001 7.

11 March 1996; accepted 22 April 1996

Radio Frequency Signals in Jupiter's Atmosphere

L. J. Lanzerotti, K. Rinnert, G. Dehmel, F. O. Gliem, E. P. Krider, M. A. Uman, J. Bach*

During the Galileo probe's descent through Jupiter's atmosphere, under the ionosphere, the lightning and radio emission detector measured radio frequency signals at levels significantly above the probe's electromagnetic noise. The signal strengths at 3 and 15 kilohertz were relatively large at the beginning of the descent, decreased with depth to a pressure level of about 5 bars, and then increased slowly until the end of the mission. The 15-kilohertz signals show arrival direction anisotropies. Measurements of radio frequency wave forms show that the probe passed through an atmospheric region that did not support lightning within at least 100 kilometers and more likely a few thousand kilometers of the descent trajectory. The apparent opacity of the jovian atmosphere increases sharply at pressures greater than about 4 bars.

Electrical discharges in Earth's atmosphere have long been of interest to humans as cultural, scientific, and technical phenomena (*1*). Electrical discharges in the atmospheres of other planets (*2*) are important for understanding atmospheric dynamics and may be significant in producing nonequilibrium chemical processes in a planetary atmosphere (*3*). For Jupiter, it has been shown theoretically that the nonthermal radio emissions (which are easily detectable from Earth) are not caused by lightning (*4*).

Optical evidence of lightning in the nightside jovian atmosphere found by the Voyager imaging systems (*5*) and the measurement of whistler-mode waves in the jovian magnetosphere (*6*) suggested that electrical signals might be found by the Galileo probe. The lightning and radio emission detector (LRD) was designed (*7*) to be as flexible in its measuring capabilities as the probe on-board resources would allow. Many of the design decisions invoked knowledge of Earth lightning and extended the parameter limits by several factors of 10 in both directions. Because Jupiter has no well-defined surface close to the cloud system, it was believed that there would be no cloud-to-ground discharges, which are the best understood type of lightning on Earth. Cloud discharges on Earth are complex physical phenomena that generate a variety of radio frequency (RF) pulses and pulse trains (*1*).

Substantial efforts were made during probe development to reduce the electromagnetic interference (EMI) in the LRD from the subsystems in the probe. The LRD was tested during two flybys of Earth by Galileo in order to characterize the EMI noise expected during atmospheric entry. The acquired data demonstrated that only the net flux radiometer (NFR) (*8*) produced

L. J. Lanzerotti, Bell Laboratories, Lucent Technologies, Murray Hill, NJ 07974, and the University of Florida, Gainesville, FL 32611, USA.

K. Rinnert, Max-Planck-Institut für Aeronomy, D-37191 Katlenburg-Lindau, Germany.

G. Dehmel, F. O. Gliem, J. Bach, Universität Braunschweig, D-38106 Braunschweig, Germany.

E. P. Krider, University of Arizona, Tucson, AZ 85721, USA.

M. A. Uman, University of Florida, Gainesville, FL 32611, USA.

*Present address: Nortel Dasa Network Systems, D-88039 Friedrichshafen, Germany.

significant EMI in the LRD, and much of this was at low frequencies. In addition, the instrument was tested on Earth lightning (9) on several occasions. The EMI signature from the NFR during the flybys and the information gained from the laboratory and field tests on Earth have been used in interpretation of the data presented here.

The LRD calibration sequence after the instrument was turned on at the beginning of the descent showed that the LRD operation was nominal. The signal amplitudes measured in the first two intervals of pressure (Fig. 1, A and B) occupied four wave form analyzer (WFA) amplitude levels, indicating magnetic fields of up to 500 nT. The counting rate in the first interval was quite high (~144,000 counts total), with so many pulses that there were no interpulse gap times >72 ms. The counts dropped by a factor of ~10 during the second interval; longer interpulse gap times, up to ~1 s, were measured. The majority of the pulse durations were near the upper limit of measurement, ~0.5 ms, during these first two intervals. The pulse amplitudes at pressures of 8.4 and 16.0 bars (Fig. 1, C and D) were <50 nT. In both intervals, the instrument switched back to its most sensitive mode, and the 3-kHz amplitude at 8.4 bars was the lowest measured during descent. The duration distributions in the vicinity of the small peak at 8 to 24 μs resemble those for the noise signals from the NFR, although the overall counting rates and amplitudes are larger (by a factor of perhaps 5 or more) than those of the noise level.

Significant anisotropies are seen in the direction of arrival of the RF signals (Fig. 2). The variation in the period of the probe spin during a measurement interval prevents identification of an arrival direction with respect to the local horizontal magnetic field. There is also a $\pm\pi$ ambiguity in the arrival direction determined by the spinning antenna. Displaying in this fashion only the largest amplitude signals and the largest and next largest amplitude signals gives similar anisotropies. With the possible exception of a distribution acquired at ~2.8 bars, all of the other measuring intervals tended to show anisotropies similar to those in Fig. 2.

Most wave forms (*10*) captured during the descent were dominated by relatively low-frequency spectral content (~500 Hz) (Fig. 3). The wave form from 1.1 bars (Fig. 3A) was the only one in the descent that was coincident with an optical fluctuation. Of the 544 optical events that were counted in this interval, 320 were coincident with a wave form. A high, thin cloud was detected by the probe nephelometer (*11*) at this pressure interval. It is probable that the coincidence of the photodiode (OPT) signal with a wave form was accidental. Although the wave form is not a perfect sinusoid, a sine wave fit shows a dominant frequency of ~725 Hz. Although a sinusoid cannot be fit to the other wave forms in Fig. 3, several others measured during descent do resemble partial sine waves, similar to some signals detected during the Earth flybys. The quasi-sinusoidal wave forms during the descent had much larger amplitudes than any recorded during the Earth flybys. It has not been possible to determine if the NFR caused these wave forms and, if so, how they are produced in that instrument because no similar NFR frequencies have been identified. The second wave form (Fig. 3B), acquired below the thin cloud layer at 2.1 bars, was the largest signal detected in the descent. The fourth wave form (Fig. 3D) was the last acquired in the descent (at a pressure of 16 bars) and is characterized by a relatively high dominant frequency of ~5 kHz.

Figure 4 shows the RF amplitudes (pow-

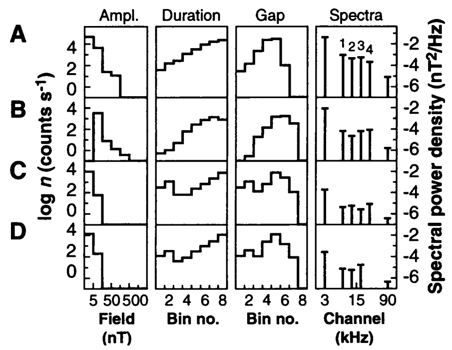

Fig. 1. Statistics measured for the RF signal quantities in four selected pressure measuring intervals: (**A**) 0.7 to 1.5 bars; (**B**) 1.5 to 2.5 bars; (**C**) 7.6 to 9.3 bars; and (**D**) 15.0 to 17.3 bars. The columns correspond to the amplitude, duration, and gap time (or interpulse) distributions. The scale on the left is for these three leftmost distributions. The rightmost column contains the integrated amplitudes of the signals measured during the intervals in each narrowband channel: 3, 15, and 90 kHz. The four amplitudes for the 15-kHz channel (labeled 1 through 4) correspond to the amplitudes in each of the four directionally sectored channels (each multipled by 4 to give a comparison with the other two channels). Total counts and bin sizes are in (*18*).

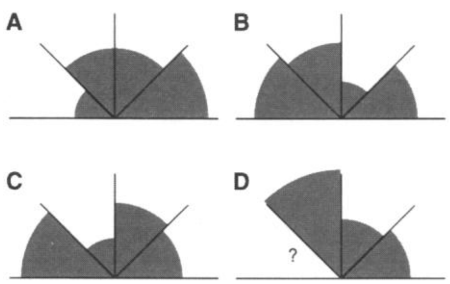

Fig. 2. Directional distributions of the signal occurrences in the 15-kHz narrowband channel for the four pressure intervals in Fig. 1: (**A**) 0.7 to 1.5 bars; (**B**) 1.5 to 2.5 bars; (**C**) 7.6 to 9.3 bars; and (**D**) 15.0 to 17.3 bars. The instrument measures four sectors but cannot distinguish in which direction the local field is pointing. Each plot is normalized to the sector-summed power density in the measuring interval, giving the same total gray area in each plot. The occurrences recorded in each sector are proportional to the sector area.

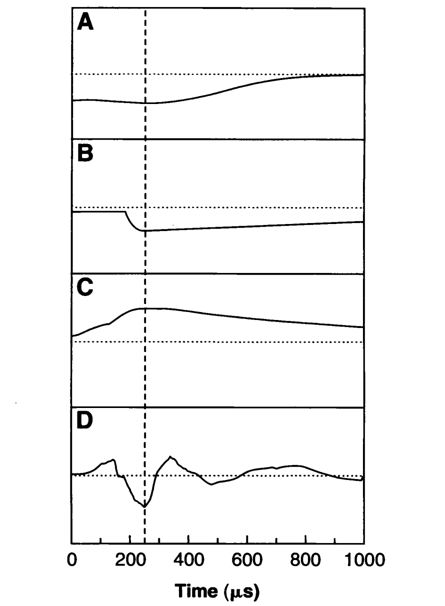

Fig. 3. Wave forms measured by the WFA during the four pressure intervals in Figs. 1 and 2. In each panel, the dotted line across the center is the zero amplitude line. The WFA trigger point is the vertical dashed line at 250 μs. The maximum signal amplitudes from the zero amplitude lines are (**A**) 32.2 nT, (**B**) 412.5 nT, (**C**) 37.5 nT, and (**D**) 32.8 nT.

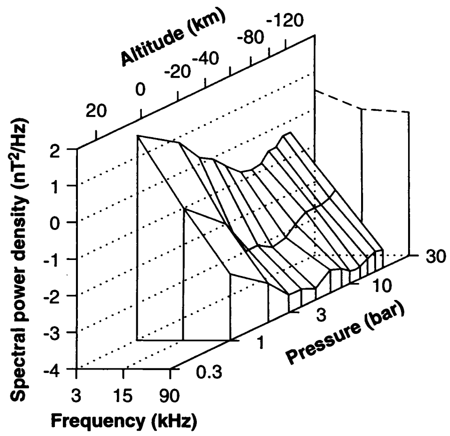

Fig. 4. Plot of the spectral power density (log values) measured in each narrowband frequency channel (3, 15, and 90 kHz) as a function of atmospheric pressure during probe descent into the atmosphere. The corresponding atmospheric depth is shown along the top axis. The amplitudes in the 15-kHz channel correspond to the sector-summed amplitudes. The power levels at 30 bars (dashed line) show a typical LRD response to a close (~20 km) thunderstorm on Earth.

er densities) in the three narrow band frequency channels versus increasing pressure, or equivalently depth or time. The jovian spectrum is concentrated in the low-frequency (3 kHz) band (Fig. 4), consistent with the statistics in Fig. 1 and the wave forms in Fig. 3. At pressures greater than ~3 bars, the 90-kHz values are at the instrument background level. Both the 3- and the 15-kHz amplitudes begin to increase slowly below about the 5-bar level, continuing to the end of the mission.

The opacity of the jovian atmosphere measured by the OPT did not change substantially from the initial measurement at about 1 bar to ~5 bars (Fig. 5). Below ~5 bars, the atmosphere rapidly became darker such that at the end of the mission, the light level was ≲0.01% of that at the beginning of LRD measurements. The sharp increase in opacity below ~5 bars (about the same depth at which the RF signal amplitudes began to increase) is not believed to be due to a crossing of the terminator by the probe, which should have occurred some 15 min later than when the increase began. The reason for this significant increase is unknown. Perhaps there were optically thick clouds near 5-bar pressure.

Model-ray tracings show that direct line-of-sight propagation occurs in the jovian atmosphere to distances on the order of 10^4 km (*12*). Observations beyond this distance require one or more reflections off of the ionosphere. The wave form measured at the depth of 16 bars (Fig. 3D), with an amplitude of ~30 nT, is similar in amplitude to Earth lightning (current $I \sim 10^4$ A) at a distance of 50 to 100 km. It has the appearance of distant Earth lightning that has experienced multiple ionospheric reflections. If the source of this signal is jovian lightning at a distance of ~1000 km, then $I \sim 10^5$ A. The wave form detected at 2.1 bars with an amplitude of ~400 nT (Fig. 3B) has a magnetic field discontinuity whose rise time is a factor of 10 greater than those of typical discontinuities observed in Earth lightning. A change in magnetic field in 50 μs implies a radiating source of order 10 km in dimension.

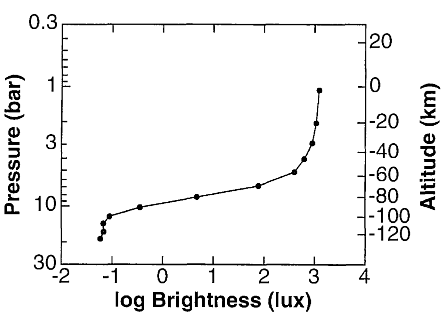

Fig. 5. Atmospheric opacity, measured with the two-photodiode OPT system, as a function of atmospheric depth.

It may be misleading to compare the rate of RF signals detected by the LRD in the jovian atmosphere to Earth atmospheric electrical discharges because, with the exception of the wave form at 16 bars, the measured jovian signals differ drastically from those on Earth. Furthermore, we do not know the mechanisms that produce the jovian RF signals. Just as recent discoveries related to Earth lightning have now identified phenomena connecting Earth's clouds to the lower ionosphere (*13*), it is possible that some jovian atmospheric electrical processes are quite different than any theorized. Given these caveats, it is known that on Earth, worldwide lightning produces ~100 total flashes per second, or equivalently, ~6 flashes km^{-2} $year^{-1}$ (*1*). If the RF signal counting rates of the LRD during the descent are corrected for known probe RF noise (which principally originates from the NFR instrument), and the direct line-of-sight detection distance is used as the effective operative radius of the LRD, then the number of jovian signals seen would be about 1/10 the number of equivalent Earth discharges in an equal area. Also, making reasonable assumptions about the source distances, the jovian discharge currents are somewhat larger than typical discharge currents in Earth lightning. Finally, the rate of any electrical discharges in the area of sensitivity of the LRD is not very different from the minimum flash rate (~0.13 km^{-2} $year^{-1}$) derived (*14, 15*) from analysis of Voyager optical data in a band around 49°N jovian latitude, where the majority of the reported optical bright spots seem to be located. The LRD rate is far less than the maximum rate derived (*16, 17*) under other assumptions of flash energy and observability (perhaps as high as 40 km^{-2} $year^{-1}$).

REFERENCES AND NOTES

1. M. A. Uman, *The Lightning Discharge* (Academic Press, New York, 1987); R. H. Golde, Ed., *Lightning* (Academic Press, New York, 1977).
2. K. Rinnert, in *Handbook of Atmospheric Electrodynamics*, H. Volland, Ed. (CRC Press, Boca Raton, FL, 1995), pp. 27–60; L. J. Lanzerotti, K. Rinnert, E. P. Krider, M. A. Uman, in *Time-Variable Phenomena in the Jovian System*, M. J. S. Belton, R. A. West, J. Rahe, Eds. (NASA SP-494, Washington, DC, 1989), pp. 374–383.
3. For example, C. Sagan *et al.*, *Nature* **213**, 273 (1967); A. Bar-Nun, *Icarus* **24**, 86 (1975); R. G. Prinn and T. Owen, in *Jupiter*, T. Gehrels, Ed. (Univ. of Arizona Press, Tucson, 1976).
4. V. V. Zheleznyakov, *Radio Emission of the Sun and Planets* (Pergamon, Oxford, 1970).
5. For example, A. F. Cook, T. C. Duxbury, G. E. Hunt, *Nature* **280**, 794 (1979); (*15, 17*).
6. F. L. Scarf, D. A. Gurnett, W. S. Kurth, *Science* **204**, 991 (1979).
7. L. J. Lanzerotti *et al.*, *Space Sci. Rev.* **60**, 91 (1992). The central detection element of the LRD instrument is a ferrite-core antenna about 32 cm long and 0.6 cm in diameter. The antenna covered a frequency range of ~10 Hz to ~100 kHz. The output of the antenna provides the input signal for three principal RF data channels: (i) the WFA for statistics of wave form characteristics and snapshots (in a 1-ms time window), (ii) the spectrum analyzer, which consists of three narrowband channels having central frequencies of 3, 15, and 90 kHz and the highest sensitivity of all the instrument channels, and (iii) a dc channel that determines the probe spin rate and the magnetic field intensity in the spin plane of the probe. Two photodiodes (OPT), each mounted behind a fisheye lens and located on opposite sides of the probe aft shelf, provides data on both the opacity of the atmosphere with depth and transient fluctuations in light levels. Each data accumulation interval was ~4 min. Statistics data were returned for 12 accumulation intervals during the descent; only the first 11 recorded wave forms were returned before probe failure.
8. L. A. Sromovsky *et al.*, *Science* **272**, 851 (1996).
9. L. J. Lanzerotti *et al.*, *J. Geophys. Res.* **94**, 13221 (1989); K. Rinnert *et al.*, *ibid.* **90**, 6239 (1985).
10. The WFA used two parallel pipeline memory systems to continually sample and store the RF signals in each measuring interval. The signal stored and transmitted during each measuring interval was based on a priority scheme established before flight, with the highest priority given to the largest amplitude wave form that might be coincident with an optical fluctuation. The next highest priority was accorded to the largest wave form without an OPT signal. One interval during descent was devoted to the capture of the last 1 ms measured (a so-called "random" waveform).
11. B. Ragent, D. S. Colburn, P. Avrin, K. A. Rages, *Science* **272**, 854 (1996).
12. K. Rinnert *et al.*, *J. Geophys. Res.* **84**, 5181 (1979).
13. R. C. Franz, R. J. Nemzek, J. R. Winckler, *Science* **249**, 48 (1990); D. D. Sentman and E. Westcott, *Geophys. Res. Lett.* **20**, 2857 (1994).
14. L. R. Doyle and W. J. Borucki, in *Time-Variable Phenomena in the Jovian System*, M. J. S. Belton, R. A. West, J. Rahe, Eds. (NASA SP-494, Washington, DC, 1989), pp. 384–389.
15. W. J. Borucki and J. A. Magalhaes, *Icarus* **96**, 1 (1992).
16. M. A. Williams, thesis, Univ. of Arizona (1986).
17. ———, E. P. Krider, D. M. Hunten, *Rev. Geophys.* **21**, 892 (1983).
18. Counting statistics: (A) 144,247 counts in 194.7 s, gain 3; (B) 12,163 counts in 260.6 s, gain 2; (C) 41,453 counts in 260.4 s, gain 3; and (D) 63,656 counts in 252.6 s, gain 3. Instrument gain ranges from 0 (least sensitive) to 3 (most sensitive). Bin ranges are in microseconds. Duration distribution bins: 1, <8; 2, 8 to 24; 3, 24 to 40; 4, 40 to 72; 5, 72 to 138; 6, 138 to 256; 7, 266 to 522; 8, >522. Gap time distribution bins: 1, <8; 2, 8 to 40; 3, 40 to 168; 4, 168 to 680; 5, 680 to 8,700; 6, 8,700 to 72,200; 7, 72,200 to 1,100,000; 8, >1,100,000.

19. This binational collaborative project would not have been possible without the enthusiastic support and help of numerous individuals in both Germany and the United States over two decades. W. I. Axford, Director of the Max-Planck-Institut für Aeronomy, was the original stimulant for the investigation and provided encouragement over the many years. We thank the Galileo Project Office at NASA Ames for its assistance throughout the program, especially B. Chin, A. Wilhelmi, C. Sobeck, M. Smith, R. E. Young, P. Melia, J. Sperans, and N. S. Vojvodich. The help of the Hughes organization under the management of U. Lapins was critical for solving many technical issues. We especially thank M. Zadow (University of Braunschweig) and G. Umlauft (Max-Planck-Institut für Aeronomy) for their technical assistance and design advice. The technical staff of Dornier Systems, Friedrichshafen, was responsible for the construction of the final flight unit. We thank Y. Su and V. Rakov (University of Florida) for assistance in tests of the LRD and C. G. Maclennan (Bell Laboratories) for help over the years with data evaluations from tests and the descent. This collaborative program was supported in Germany by Deutsche Agentur für Raumfahrtangelegenheiten grant 50 QJ 9005 and in the United States by NASA Ames Research Center contract NAG 2-667 with the University of Florida.

7 March 1996; accepted 18 April 1996